

Scientific Report and Bibliography of the Group of
A. Zensus

1997–1999

Active galactic nuclei, compact radio sources and VLBI

1 Summary of research activities

The main aim of the research carried out by the group is to gain insight into the phenomena associated with Active Galactic Nuclei (AGN). In the radio domain, these are mainly associated with spectacular collimated outflows, or “jets”, originating deep in the “radio nuclei”. The study of these regions requires high resolution, now better than 0.1 milliarcsec through the use of millimetre- and space-VLBI and high sensitivity, since the intrinsic luminosity of AGN ranges over at least 10 orders of magnitude. The high luminosity and activity (variability in flux and structure) of quasars, BL Lacertae objects and other kinds of AGN are thought to be caused mainly by the accretion of matter onto super-massive black holes. At present the processes which lead to the ejection of highly relativistic material and its subsequent confinement into jets are not yet fully understood and need to be investigated in more detail.

The relativistic jet model successfully explains most of the observed properties of the jets in terms of shocks in the outflowing material. The basic assumption of this model is that the radio emission is produced by the synchrotron mechanism. One consequence of this is that the radio brightness temperature T_b , in the rest-frame of the emitting plasma, cannot significantly exceed $\sim 10^{12}$ K, because of the resulting Inverse-Compton cooling. Recent observations, *e.g.* directly by means of space-VLBI, or from measurements of Intraday variability (IDV) show, however, that this limit can be exceeded by one (space-VLBI) to several (IDV) orders of magnitude. In the latter case, even if the rapid variability is caused by scattering in the interstellar medium, $T_b \sim 10^{15}$ K; if it is intrinsic to the source, $T_b \sim 10^{20}$ K. The group has been active in observing these phenomena, as well as in using theoretical models to disentangle the intrinsic and extrinsic contributions to the Intraday variability.

Millimetre-VLBI provides the highest resolution possible with Earth-based arrays and also permits deeper probing of the central, self absorbed regions of AGN. Space-VLBI can, in principle, provide an even higher resolution and can also allow direct measurement of radio brightness temperatures higher than 10^{12} K. A combination of both these techniques has been used by the group to investigate the kinematics of the jets in AGN. Important are measurements of not only total intensity, but also of polarization, which permits the mapping of the magnetic fields in the inner regions of AGN. Also important are concurrent observations in several regions of the electromagnetic spectrum, to study the correlations between the activity in the radio, optical and γ -ray domains. Such investigations have traditionally been a major

activity of the group.

AGN are not only very interesting objects of study in their own right, but are also powerful tools for astrometry. The spacing between reference points in radio sources as far as 15° apart can currently be measured with an accuracy better than 0.1 milliarcsec using VLBI phase-connection techniques. Such measurements have been made and the determination of an inertial frame independent of the motion of the vernal equinox is within sight.

Gravitationally lensed objects have also been studied. The gravitational lens effect occurs when the gravitational field of an intervening object (galaxy) distorts the radiation from a distant object. Typically, 2 or 4 detectable images are produced, each of which is a scaled and distorted image of the background source. VLBI polarimetry provides a powerful tool for investigating gravitational lens images, since the degree and angle of linear polarisation are unchanged by the lens process itself. This provides a constraint on the mass distribution of the lensing object. Quadruple ("Quad") systems are of particular interest, since they provide magnifications of intrinsic motions in the source by factors of 10–100.

Finally, as an example of a low-energy AGN and the nearest black-hole candidate, the radio source Sagittarius A* which lies at the dynamical centre of our Galaxy has been studied, both by millimetre-VLBI and theoretically.

2 Sub-milliarcsecond structure: millimetre and space VLBI

The high luminosity and activity (variability in flux and structure) of quasars, BL Lacertae objects and other kinds of AGN are thought to be caused mainly by the accretion of matter onto super-massive black holes. At present the processes which lead to the ejection of highly relativistic material and its subsequent confinement into jets are not well understood and need to be investigated in more detail. Millimetre-wave interferometry with transcontinental baselines (hereafter: mm-VLBI) provides a powerful tool for this kind of research.¹ The advantages of mm-VLBI are twofold: first, it allows imaging with an angular resolution higher than any other Earth-based method, and second, regions which are self-absorbed (or in the case of Sgr A* scattered) at longer wavelengths can be imaged directly.

2.1 AGN at high resolution

The group has been active in global Coordinated Millimeter VLBI Array (CMVA) observations performed between 1996 and 1999 (typically 2 experiments per year), the most recent of which involved 12 antennas. At 86 GHz, images of high quality can now be made as illustrated below.

Fig. 1 shows a new 86 GHz map of the highly active and superluminal quasar 3C454.3 ($z = 0.859$). At longer wavelengths, the source has been well studied (see section 3.5).

Those observations revealed relatively high superluminal velocities on scales of mas to tens of

¹In the following: 1 mas (milliarcsec) = 10^{-3} arcseconds; the Hubble constant $H_0 = 100 \text{ km s}^{-1} \text{ Mpc}^{-1}$, $q_0 = 0.5$

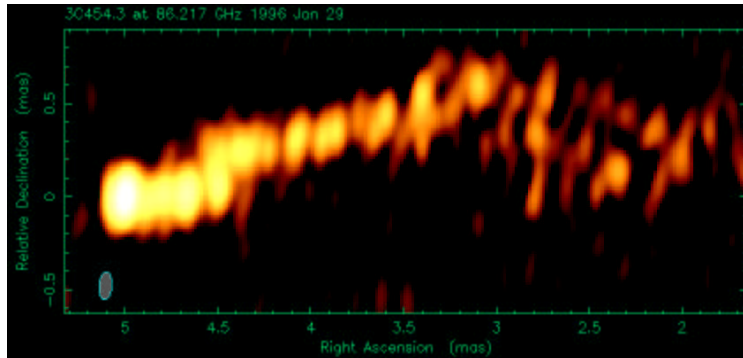


Figure 1: 86 GHz VLBI map of the jet of the highly active blazar 3C 454.3, revealing details as small as 1 light year. The observations were made in Jan 1996 using an array of 3 European and 3 US stations. The dynamic range of the map is $\sim 200:1$, a factor of 2-3 higher than that of images made in 1993/1994.

mas ($\beta_{app} \sim 20$).² The maps at 86 GHz now reveal motion of $\beta_{app} = 5 - 7$, which is slower, but consistent with that found earlier in the core region (Nat 328, 778, 1987). With an observing beam size of only $70 \mu\text{as}$ ³, details in the jet corresponding to a spatial resolution of 0.3 pc can be observed and the jet seems to become resolved transversely. The mean ridge line of the jet shows bends, wiggles and displacements (kinks), much resembling Kelvin Helmholtz instabilities in a relativistic hydrodynamical flow, such as are also observed in other sources at longer λ and on larger scales. Future mm-VLBI imaging and monitoring of the structural changes will give new insight on the details of these quite complex jet physics (*e.g.* for studies of the evolution of instability modes with time), and will help to answer questions about jet stability and confinement in the presence of ‘jet-disrupting’ instabilities as well as on the dynamical importance of jet-stabilizing magnetic fields.

People involved: D. Graham, A. Kraus, T.P. Krichbaum, I.I.K. Pauliny-Toth, A. Witzel, J.A. Zensus

Collaborators: H. Ungerechts, A. Greve, M. Grewing (IRAM), J. Wardle (Brandeis), A. Marscher (Boston Univ.)

The FRII radio galaxy Cygnus A has been studied with VLBI at 1.6, 22 and 43 GHz (λ 18 cm, 1.3 cm and 7 mm). The new maps (Fig. 2) show the jet and counter-jet of Cygnus A on scales from ~ 400 to 0.1 mas, *i.e.* on projected sizes of ~ 300 pc to 0.07 pc. The best 22 GHz image shows a few degrees of misalignment between the VLBI-jets and the kpc-jets, longitudinal oscillations of the jet ridge line with amplitudes of ≤ 0.6 mas, and transverse oscillations of the jet width with amplitudes of 0.2 – 0.3 mas, both of which are consistent with Kelvin-Helmholtz instabilities.

Within 15 mas from the core, both jets expand with an opening angle of $\sim 5^\circ$. Between 22 and 43 GHz the core has an inverted spectrum. The spectrum of the jet appears steep, that of the counter-jet relatively flat. Two 22 GHz observations give evidence for apparent acceleration

² β_{app} is the ratio of the apparent velocity of motion to c , the velocity of light

³ $1 \mu\text{as} = 10^{-6}$ arcsec

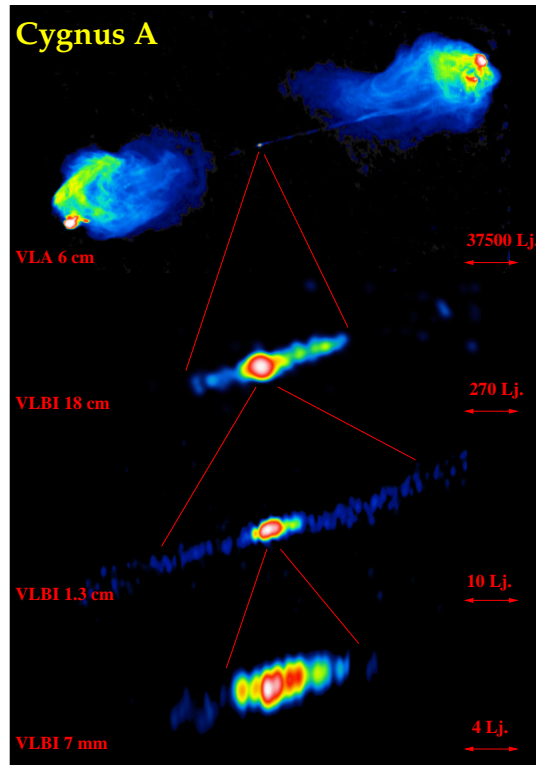


Figure 2: The jet of Cygnus A imaged at 4 different resolutions. **Top image:** VLA map obtained at λ 6 cm (ApJ, 1984, 285, L35). **Image below:** the jet imaged with the European VLBI Network (EVN) at λ 18 cm. The angular resolution is 20 mas, or 65 light years (ly). **Third image:** the innermost regions of the source at a resolution of ~ 0.4 mas (1 ly) at λ 1.3 cm. Features in the jet move with speeds ranging from 0.1 c to 0.7 c. **Bottom:** at λ 7 mm the nucleus is seen with the highest resolution so far, of only 0.15 mas, or 130 light days. The inner 7 ly of the core and the jet are seen here. The bars at the right of the images gives their spatial scales.

(from 0.1 c to 0.7 c) along the jet, which could be jet-intrinsic or related to phase velocities. In the counter-jet structural variations also seem to be present, but cannot yet be accurately determined. Between 1.6 GHz and 43 GHz the jet-to-counter-jet ratio R is frequency dependent with a maximum of $R \simeq 5$ near 5 GHz and a lower $R = 1 - 2$ at 1.6 GHz and 43 GHz, which may be due to absorption by a partially opaque, inclined absorber (*e.g.* a disk or a torus) surrounding the nucleus and obscuring the counter-jet but not the jet. With a jet-to-counter-jet ratio corrected for such foreground absorption, the jet appears to be nearly perpendicular to the line of sight ($\theta > 80^\circ$, for $R < 2$) and its intrinsic velocity lies in the range $0.2 \leq v/c < 1$.

People involved: T.P Krichbaum, W. Alef, A. Witzel, J.A. Zensus

Collaborators: R.S. Booth, (Onsala), A. Greve, (IRAM), A.E.E Rogers (Haystack)

In early 1992 a prominent flare occurred in the S5 quasar 0836+71 ($z = 2.17$, see also 2.4, 6.2), peaking nearly simultaneously at γ -ray, X-ray and optical wavelengths, then propagat-

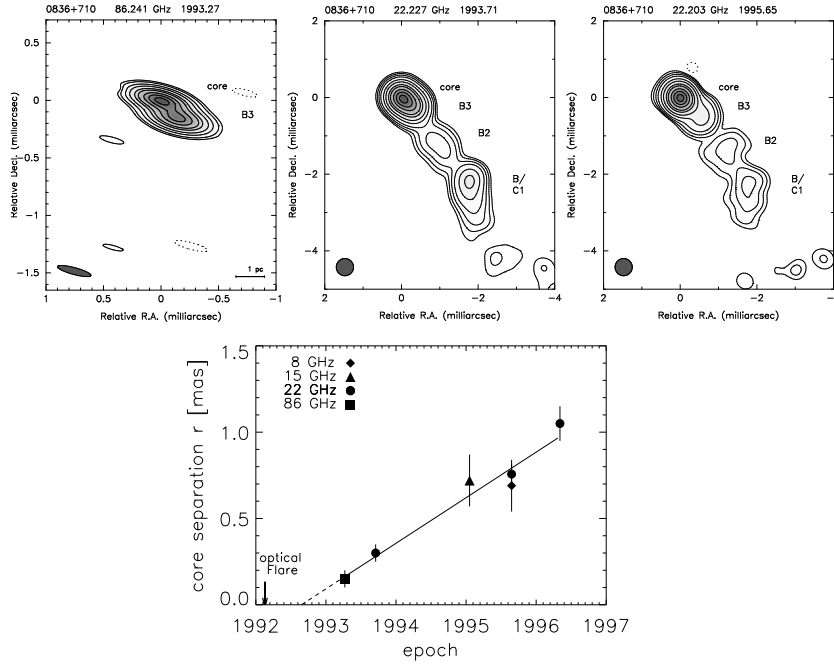


Figure 3: **Top:** 86 GHz CMVA and 22 GHz Global VLBI maps of the inner jet of the quasar 0836+710. Beam sizes are 0.30×0.06 mas at 86 GHz and 0.45 mas at 22 GHz.

Bottom: Separation of component B3 from the core vs. time. Symbols denote different frequencies as shown in the plot. The solid line is a linear fit with slope 0.26 mas/yr, *i.e.* superluminal motion with $\beta_{\text{app}} = 10.8$. Linear back-extrapolation (dashed line) yields component ejection near 1992.65. The arrow shows the onset of the optical/ γ -ray flare (1992.13)

ing into the mm–radio–bands. VLBI observations, first at 86 GHz (1993.27) and later also at lower frequencies (22, 15, 8 GHz), revealed the ejection of a new jet component separating from the core with a highly superluminal speed ($\sim 11c$). Back-extrapolation of the motion shows that this component was ejected soon after the γ -/X-ray/optical flare (Fig. 3). This finding further supports the hypothesis that broad-band flux density activity and injection of relativistic plasma at the base of the jet are tightly correlated and that the γ -ray radiation is indeed Doppler-boosted emission produced near the origin of the jet.

People involved: T.P. Krichbaum, A. Kraus, A.P. Lobanov, A. Witzel, J.A. Zensus
Collaborators: K. Otterbein, S.J. Wagner (Heidelberg), S. Britzen (Dwingeloo), C.A. Hummel, K. Johnston, (USNO, Washington)

At $\lambda 1.3$ mm (~ 230 GHz) VLBI observations with transcontinental baselines yield a beam as small as $25\mu\text{as}$. For the archetypical quasar 3C 273 ($z = 0.158$), this corresponds to a spatial resolution of 0.044pc (52 light days), or ~ 500 Schwarzschild radii R_s (for a central black hole of $10^9 M_\odot$). A probably even better candidate for studies of the direct vicinity of a supermassive black hole is the compact radio source Sgr A* at the Galactic Centre (see below).

2.2 Sagittarius A*: the black hole at the Galactic Centre

Stellar proper motion studies have unambiguously demonstrated the presence of a compact dark mass, almost certainly a black hole, of $2.6 \cdot 10^6 M_{\odot}$ in the Galactic Centre. Various arguments suggest that this mass is associated with the compact, non-thermal radio source Sgr A* which lies at the dynamical centre of the Galaxy. It is still unclear whether this source is an underfed jet or perhaps the inner region of an advection dominated accretion flow (ADAF). Because of its importance as the closest supermassive black hole candidate, this source has been at the focus of intense studies in the radio regime over the last 20 years.

With the detection of Sgr A* at 215 GHz on the 1150 km long baseline between Pico Veleta and one Plateau de Bure antenna, a first step towards the imaging of the ‘event horizon’ of a black hole was taken. In this experiment (see fig. 4), a size estimate of $17 \pm 9 R_s$ was obtained which, however, should be regarded with some caution, owing to remaining calibration uncertainties. A hard lower limit to the size of Sgr A* is set by its Schwarzschild radius, which becomes equal to the scattering size near 270 GHz. Thus future 1 mm VLBI observations with transatlantic or intercontinental baselines should allow us to determine how compact Sgr A* really is.

People involved: T.P. Krichbaum, D.A. Graham, A. Witzel, J.A. Zensus

Collaborators: A. Greve, J.E. Wink, M. Grewing (IRAM), P. de Vicente, J. Gomez-Gonzalez (Yebe), A. Baudry (Bordeaux)

Sgr A* has also been observed at λ 7 mm with the VLBA, yielding the most complete high-frequency image of this source to date. The imaging confirmed the earlier hypothesis that the black hole region is obscured by an intervening plasma cloud. It was also shown that the source is very compact, less than 4 AU in size, and with no unobscured structure to a limit of 35 mJy. These results place important constraints on theories for this object. A study of Sgr A* at λ 3 mm with the CMVA provided the first closure phase detection at this wavelength, and put important limits on the degree of structure in the source.

The linear polarization of Sgr A* was investigated with the VLA and with the BIMA. The VLA work at cm- λ reveals that the source is unpolarized to a level of 0.1%. Employing a novel spectropolarimetric method, a search was also made for very high rotation measures (RM) in the direction of Sgr A*. Such a high RM would effectively depolarize a signal in a standard continuum observation. No linear polarization was detected to a limit of 0.3% for RM as high as 10^7 rad m^{-2} . The BIMA work at mm- λ is one of the first attempts to measure polarizations at high frequencies and yielded an upper limit of 1% to the linear polarization at 86 GHz. Surprisingly, however, Sgr A* was found to be **circularly** polarized at a relatively high level between 0.7%-0.2% from 1.4 to 8 GHz –important information that had been missed so far. How a compact radio core can have a significantly higher circular than linear polarization is not yet understood, making Sgr A* a unique object among known radio nuclei.

People involved: G. Bower, H. Falcke

Collaborators: D.C. Backer, M.C.H. Wright (Berkeley), W.M. Goss (NRAO), J.-H. Zhao (CfA Harvard)

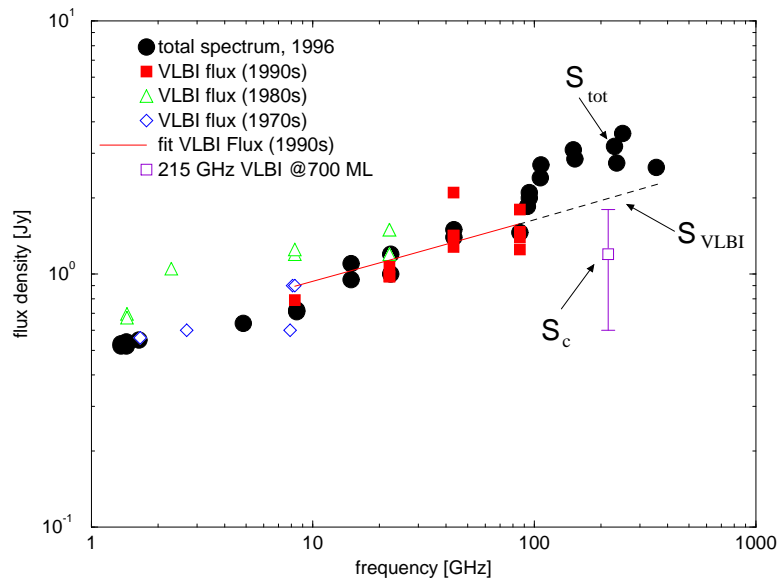


Figure 4: The cm- to mm-spectrum of Sgr A*. Filled black circles show the total flux S_{tot} . Fluxes of the VLBI component (S_{VLBI}) at 3 arbitrarily binned time intervals are shown by: filled red squares for the 1990s, open green triangles for the 1980s and open blue diamonds for the 1970s. The solid line shows a power-law fit to the VLBI spectrum of the 1990s ($S_{\text{VLBI}}[\text{Jy}] = 0.535 \cdot \nu^{+0.24}$ where ν is the frequency in GHz), which compares well with the total spectrum. For $\nu > 100$ GHz the difference between total flux and extrapolated spectrum (dashed line) indicates a flux density excess. At 215 GHz a correlated flux of $S_c = 1.2 \pm 0.6$ Jy was measured (open square). The source size is $50 \leq \theta \leq 190 \mu\text{as}$.

Sgr A* was also studied theoretically. Simplified equations for a freely expanding, pressure driven jet model were successfully applied to the radio cores in the black hole candidates GRS1915+105, NGC4258, M81, and Sgr A*. The jet powers derived from this almost parameter-free model are comparable to the accretion disk luminosities attributed to these systems. This provides further evidence for the existence of symbiotic jet/disk systems and a common engine mechanism also in low-luminosity AGN and stellar mass black holes. With the exception of Sgr A* an ADAF model seems unnecessary to explain any of the radio cores which span a large range in luminosity and size, as well as in black hole masses and accretion rate. It appears that the jet model can be used to derive minimum accretion rates and that Sgr A* is radiatively deficient in the optical range, so that a combination of a jet and ADAF model may be one possible solution.

People involved: H. Falcke

A major problem in studying the structure of Sgr A* with VLBI is that it is scatter-broadened at all wavelengths up to the mm-regime. On the other hand, the resolution of mm-VLBI today is already down to a few tens of the Schwarzschild radius. To investigate whether mm-VLBI can eventually study general relativistic effects, computer simulations of the black hole in the Galactic Centre were made with a general relativistic ray-tracing code.

It was shown that for arbitrary morphologies of the emission region one will always see a well-defined cavity (the “hole”) at submm-wavelengths caused by the photon horizon. Irrespective of the spin of the black hole this cavity will have a size of $30 \pm 3 \mu\text{as}$. Considering the effects of interstellar scattering and the finite telescope resolution one can show that at $\lambda < 1 \text{ mm}$ this cavity (Fig. 5), which must be present if Sgr A* does contain a black hole, should be detectable with submm-VLBI arrays within the next one or two decades. Such an observation would, for the first time, allow one to directly image the event horizon of a black hole, which would be of fundamental importance for physics in general.

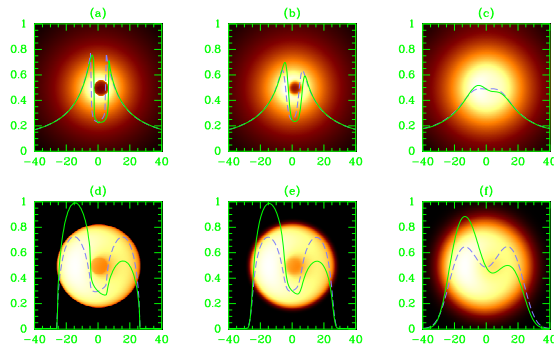


Figure 5: A simulated image of the compact emitting region around a black hole with the characteristics of Sgr A* at the Galactic Centre. The black hole is here either maximally rotating (panel a-c) or non-rotating (panel d-f). The emitting gas is assumed to be in free fall (top) or on Keplerian orbits. The viewing angle is 45° . Panels a&d show the result of the general relativistic ray-tracing calculation, panels b&e the same figure as seen by a VLBI array at $\lambda 0.6 \text{ mm}$ taking interstellar scattering into account, and panels c&f the same at $\lambda 1.3 \text{ mm}$. The intensity profiles in the x - (green) and y -directions (purple) are overlaid. The axes are the intensity in arbitrary units and the distance from the black hole in R_g which for Sgr A* is $3.86 \times 10^{11} \text{ cm} \sim 3 \mu\text{as}$. The central “hole” in this case is therefore expected to have a diameter of $\sim 30 \mu\text{as}$.

People involved: H. Falcke

Collaborators: F. Melia (Steward Observatory), E. Agol (John Hopkins)

2.3 Millimetre outbursts and IR/ γ -ray flares

Between 1991 and 1993 two mm-radio outbursts, associated with two γ -ray flares were observed in the source 0528+134. The “burst injection model” was used to analyse the outbursts and could explain the light-curves in the wide frequency range of 2.3 to 150 GHz. The evolutionary relationship between the γ -ray flares and the associated mm-wave outbursts was also investigated. It was shown that the spectral tracks of the mm outbursts and the γ -ray flares do not directly connect. In the submm-mm waveband, there may be two components: one related to the γ -ray flare which evolves from optically thick to optically thin and one, a purely mm-wave outburst which is optically thin from the beginning.

People involved: S.J. Qian, A. Witzel, T.P. Krichbaum, A. Kraus
Collaborators: S. Britzen (Dwingeloo), E.B. Waltman (NRL), E. Valtaoja (Metsähovi),
H.D. Aller (Univ. Michigan)

The continuous spectral evolution of IR–mm flares in blazars has been analysed in terms of the "shock-in-jet" model. It was shown that the rising phases of flares are closely related to the behaviour of the transition from the Compton stage to the synchrotron stage and that bulk acceleration of the IR–mm blobs during the transition must be taken into account.

People involved: S.J. Qian, A. Witzel, T.P. Krichbaum, A. Kraus, J.A. Zensus
Collaborators: X. Zhang (BAO, Beijing)

2.4 Ground-based and space-VLBI study of the parsec-scale jet in 0836+710

The parsec-scale jet in the luminous quasar 0836+710 ($z = 2.17$, see also 2.1, 6.2) has been studied and a set of jet parameters which can explain several observed properties of this object has been obtained: the spectral evolution of total radio emission; the time delay between γ -ray and radio flares; the morphology and kinematics of the jet on scales of up to ~ 1 kpc. High frequency VLBI-observations started in 1992, after a strong γ -ray flare, revealed the appearance of a new jet feature ejected shortly after the outburst. Monitoring of the total radio spectrum permitted the detection of a synchrotron self-absorbed spectral component consistent with emission from an adiabatically expanding relativistic shock. This component has been identified with the ejected jet feature, allowing the modelling of the time lag between the outburst and the ejection of the jet feature. The model predicts that the jet radio-core is separated by $r_{\text{core}} \approx 15$ pc from the jet base. The jet plasma has a bulk Lorentz factor $\gamma_j \approx 12$, and moves at an angle of about 3° to the line of sight. The jet opening angle derived from the expansion of the spectral component is $\phi_j = 2.1^\circ$.

These parameters also explain the observed structure and kinematics of the jet. The latter are characterized by a wide range of speeds ($\beta_{\text{app}} \sim 1\text{--}15c$) at different locations in the jet. The complex morphology of the jet is evident in the high-resolution space VLBI⁴ image of 0836+710 shown in Fig. 6. The ridge line of the jet can be reproduced by the fastest growing spatial mode of Kelvin–Helmholtz instabilities developing in a relativistic outflow with the parameters described above and a Mach number of $M_j \approx 6$. This M_j permits the prediction of the speeds along the jet. The agreement between the predicted and measured speeds seen in Fig. 6, right panel, demonstrates the self-consistency of the above description of physical conditions in the jet.

People involved: A.P. Lobanov, A. Kraus, T.P. Krichbaum, A. Witzel, J.A. Zensus
Collaborators: K. Otterbein (Heidelberg), C. Hummel, K. Johnston (USNO)

⁴in this and the following, space VLBI refers to the Japanese VSOP mission; the orbiting satellite is named HALCA. A "VSOP" image implies ground baselines as well as ground-HALCA baselines; a "HALCA" image implies ground-HALCA baselines only.

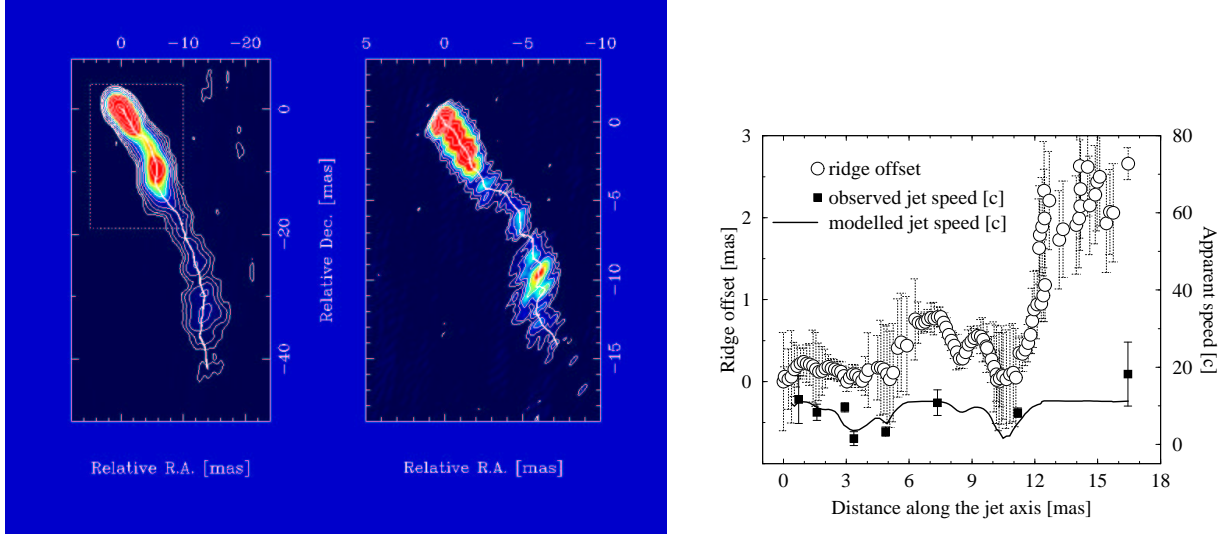


Figure 6: **Left panel:** Ground array (left) and VSOP (right) images of 0836+710, with the jet ridge line marked. In the former, the dotted rectangle shows the area covered by the VSOP image. The ground array image: restoring beam $\theta=2.2\times 1.8$ mas; contour levels are $-0.7, 0.7\times 2^n$ mJy/beam; the peak flux density $S_p=918$ mJy/beam. The VSOP image: $\theta=0.9\times 0.3$ mas; contours are $-1.5, 1.5\times 2^n$ mJy/beam; $S_p=432$ mJy/beam.

Right panel: Relation between the morphology and kinematics of the jet in 0836+710. Circles mark the offsets of the ridge line from the mean jet axis (P.A. $=-146^\circ$). Solid line: jet speeds predicted from the measured offsets; filled squares: measured speeds.

2.5 VSOP monitoring of 3C 273

The quasar 3C 273 is being monitored at high resolution with VSOP. The image obtained from the first observing epoch in December 1997 (Fig. 7) shows remarkable deviations of the transverse emission distribution from a Gaussian shape, owing to the high resolution of 0.7 mas in the direction perpendicular to the jet axis. The transverse profiles of the jet brightness plotted in Fig. 7 suggest the presence of up to 3 different emission components in the jet plasma. It is possible that the stronger central component is produced by a shocked plasma embedded in an underlying flow with the Kelvin-Helmholtz instabilities revealed in the two weaker emission components. Further VSOP observations should help in making firmer conclusions on this issue. Measuring the changes of the relative contributions from the emission features along the jet should also make it possible to determine whether helical or elliptical instability modes are dominant in the underlying plasma. Another possibility that can be further explored with the VSOP monitoring is the role of entrainment in the formation of the weaker emission features and the relation between the pc- and kpc-scale jet in 3C 273.

People involved: A.P. Lobanov, J.A. Zensus

Collaborators: Z. Abraham, E. Carrara (University of Saõ Paulo), S.C. Unwin (JPL), H. Hirabayashi, T. Bushimata (ISAS, Japan)

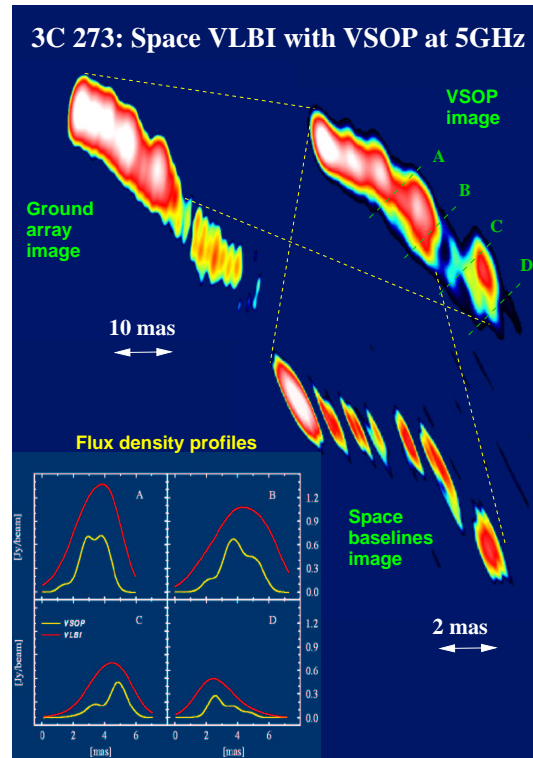


Figure 7: Ground VLBI (left), VSOP (right), and HALCA (bottom right) images of 3C 273. The HALCA image was made using only the ground–space baselines to show the reliability of the satellite data. In the inset panel, the transverse profiles of the jet brightness are shown for the VLBI and VSOP images, at locations marked in the VSOP image. The jet is transversely resolved in both images and the deviations from a Gaussian shape suggest that up to 3 emission components in the plasma are present.

2.6 Space VLBI observations of a blazar with a high brightness temperature

The blazar NRAO 530 has been observed with HALCA and an Australo-Pacific ground array at 1.6 and 5 GHz. Both images are significantly scatter-broadened by the interstellar medium. Further, these observations clearly reveal that NRAO 530 has a radio brightness temperature of $\sim 3 \times 10^{12}$ K, which is significantly higher than the limit set by the Compton catastrophe. This is very strong evidence for relativistic motion of plasma in a jet that is pointed in the direction of the Earth. The observations pose a problem for a model (ApJ 426, 51, 1994) that attributes the distribution of blazar brightness temperatures to a mechanism that maintains equipartition between the magnetic and relativistic particle energy densities.

People involved: G. Bower

Collaborators: D.C. Backer (UCLA, Berkeley)

2.7 Relative astrometry of the quasar pair 1038+52A,B

As mentioned in the previous report, ground-based VLBI studies of this quasar pair showed that the position of the “core” of quasar B, relative to that of A is frequency dependent and that much of this dependence is an effect of resolution.

In order to further investigate the interplay between resolution and spectral effects on “core” positions, this pair was observed at 1.6 GHz in November 1997 with HALCA, the VLBA and the DSN 70m antennas at Robledo and Goldstone, providing an angular resolution comparable to that obtained at 5 GHz with ground VLBI. Quasar A was well “detected” directly on Earth–Space baselines using standard fringe-fitting. The image is dominated by a compact “core” at the base of its jet, as at other frequencies.

Quasar B was well detected on all ground baselines, but could not be independently detected to HALCA. A straightforward phase-reference technique to transfer phase solutions from A was used to produce a map of B with 1 mas resolution – the first ever phase-referenced map produced with space VLBI. The image shows all 3 components which are seen in ground-only VLBI, but all are heavily resolved on the baselines to HALCA; a map made using HALCA baselines alone shows a faint response of only 10 mJy at the position of the traditional “reference” component. The position of the compact A “core”, measured with respect to the B image, is offset from the 8.4 GHz “core” position by 1.24 mas down the A jet axis. There is also a SW extension to the 1.6 GHz core which, if real, coincides with the core and knot components seen at higher frequencies.

People involved: R. W. Porcas

Collaborators: M. Rioja (JIVE)

3 Milliarcsecond to arcsecond structures

Here, the focus is on the collimated outflows (jets) originating in the radio nuclei of AGN and often extending far beyond the parent object. Of interest are superluminal motion, the geometry of the jet, accelerations and decelerations and the direction of the magnetic field. The antenna arrays used permit highly sensitive, repeatable images of the sources to be made.

3.1 Total intensity and polarimetric imaging of 3C 345

The QSO 3C 345 is a core-dominated radio source that displays apparent superluminal motions, with components travelling on the parsec-scale along curved trajectories and speeds up to $10c$. The radio source was observed with the VLBA in 1995.8, 1996.4, and 1996.8, at 22, 15, 8.4, and 5 GHz and was imaged in total and polarized intensity. A model fit was made of the inner components D (core), C8, and C7, of the jet within 3 mas of the core, yielding superluminal proper motions of $\sim 5c$ for C8 and C7. The instrumental polarisation of the VLBA antennas was calibrated, to give the feed solutions for their receivers. Images were obtained of the linearly polarized emission from the source for all epochs and frequencies.

Fig. 8 shows a composition of the total intensity, the polarized intensity and the electric vector orientation angle at 22 GHz. The electric vector is aligned with the extremely curved

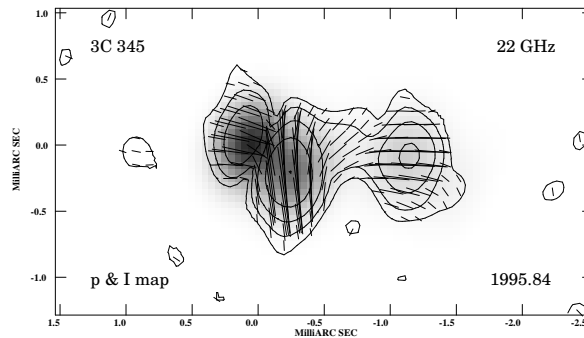


Figure 8: VLBA p , I and χ images of 3C 345 at 22 GHz, epoch 1995.84. The polarized intensity p is represented with contours (value of 7 mJy/beam \times (1,2,4,8,16), peak of brightness of 112 mJy/beam) over a grey scale total intensity map (grey scale above 7 mJy/beam) and the electric vectors (χ , length $\propto p$) superimposed over both images.

jet direction within the inner 3 mas both for the core and the C7 component. C8 is boosted in polarized emission, showing an E-vector not aligned with the jet. The polarimetric results at lower frequencies show an E-vector orthogonal to the jet direction, with remarkable emission at the edges, reaching degrees of polarization of $m \sim 15\%$ in this region at 5 GHz. The spectral analyses, including turnover frequency maps (3.2), can also provide important information on the physics of the jet, when combined with that given by the p and I -maps.

People involved: E. Ros, J.A. Zensus, A.P. Lobanov

3.2 Spectral imaging of radio emission from parsec-scale jets

This is a promising technique that permits the mapping of the synchrotron turnover frequency and turnover flux density in VLBI-scale jets. The turnover frequency ν_t is a sensitive indicator of pressure and velocity gradients arising from relativistic shocks or plasma instabilities in the jets and can be used for directly detecting the presence of the latter. The magnetic field distribution can also be reconstructed, from a combination of the ν_t and turnover flux density maps. A basic mapping method for spectral imaging has been developed and tested on the compact jets in 3C 345 (Fig. 9, left) and 3C 273 (Fig. 9, right). The map for 3C 345 shows possible locations of a relativistic channel and strong shock fronts inside the jet. The magnetic field distribution derived for 3C 273 from the ν_t and turnover flux distributions is consistent with plane shocks existing in the immediate vicinity of the source core.

The extended emission has a very low ν_t for which the existing data do not warrant a good estimate, limiting the conclusions to deducing certain information from the gradients of ν_t which are visible in the extended jet. The gradients observed in 3C 345 are reminiscent of the patterns of velocity distribution and density gradients typical for Kelvin–Helmholtz instabilities propagating in a relativistic jet. A more detailed study, with observations made at lower frequencies, is required for making conclusive statements about the nature of the observed gradients of ν_t .

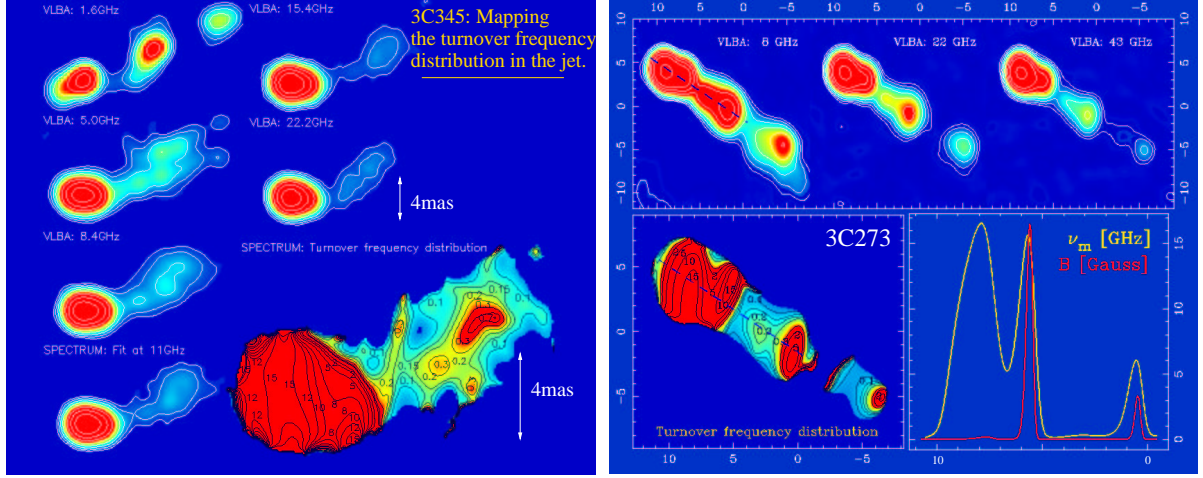


Figure 9: Turnover frequency (ν_t) mapping in the jet of 3C 345 and 3C 273.

Left, 3C 345: VLBA maps at 1.6, 5, 8.4, 15.4, and 22.2 GHz are shown; the last 4 were used to produce the ν_t distribution (the derived values of ν_t are shown by the contour levels; values below 5 GHz are upper limits). The image at 11 GHz is produced from the spectral fits, to demonstrate the feasibility of the mapping method. In the ν_t map, the core region can be well described by the emission from plane relativistic shocks. The extended jet shows indications for a possible relativistic channel (central feature extended along the jet) surrounded by a slower, possibly perturbed outflow, with signs of plasma instabilities (weaker features oriented at oblique angles with respect to the jet direction).

Right, 3C 273: The VLBA maps at 8.4, 22.2 and 43.2 GHz were used to produce the ν_t distribution (the derived values are shown next to the contour levels; the values below 8 GHz are upper limits). The ν_t profiles plotted in the inset panel are measured along the dashed line shown in the 8 GHz and ν_t images. The derived magnetic field profile peaks sharply at the location of strong jet features, indicating the likely shock origin of the latter.

People involved: A.P. Lobanov, J.A. Zensus

Collaborators: Z. Abraham, E. Carrara (University of Saõ Paulo).

3.3 Ultracompact jets as probes of central regions in AGN

The properties of ultracompact jets in several prominent radio sources (Cygnus A, 3C 309.1, 3C 345, 4C 39.25, Mkn 501 and others), are being studied using the frequency dependence of the observed position of the optically thick jet core. Frequency dependent offsets of the core positions are used for calculating the luminosities, magnetic fields, and geometrical properties of the jets.

Pressure and density gradients in the jets and in the surrounding ambient medium are the primary factors determining the observed properties of ultracompact jets. The opacity changes along these can be used for evaluating the physical conditions in them, bringing an interesting connection to studies of the environment inside and around the broad-line regions of AGN (Fig. 10).

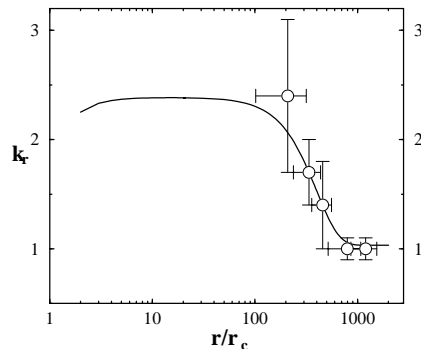


Figure 10: Opacity in the jet of 3C 309.1 reflected in the dependence of the location, r , of the optically thick VLBI core on the observing frequency, ν : $r \propto \nu^{-1/k_r}$. Circles are the measured values of k_r at different ν ; the linear scale is normalized by the distance, r_c , at which the jet becomes supersonic. The solid line shows changes of k_r due to free-free absorption in a dense nuclear region (possibly, the BLR) modelled by gaseous clouds supported by thermal pressure and maintaining a mass distribution with spherically symmetrical gravitational potential.

People involved: A.P. Lobanov

Collaborators: L.I. Gurvits (JIVE), M. Rioja (IRA Bologna)

3.4 CSO — very young radio galaxies

Compact Symmetric Objects (CSOs) have a radio structure very similar to classical double sources (FR II), but on a scale ~ 1000 smaller. Multi-epoch global 5 GHz VLBI studies of three classical CSOs: 0710+439 (see Fig. 11, left), 0108+388 and 2352+495 have led to an important discovery about this class. An increasing separation of $\sim 0.2 h^{-1} c$ between hot spots was detected in all three CSO sources studied (e.g. in 0170+439 see Fig. 11, right). For the first time, the rate of expansion in CSOs has been measured directly, showing that CSOs are very young sources, with kinematic ages of $\sim 10^3$ yrs.

As CSOs represent $\sim 10\%$ of sources in flux limited surveys, and since they are also very young, fairly rapidly growing sources, the evolutionary hypothesis of “frustrated” sources could be rejected. Nevertheless, there are still two possible scenarios of the nature of CSOs. The simplest is that they evolve via Medium-size Symmetric Objects into Large-size Symmetric Objects with decreasing luminosity with age. (A&A 106, 21, 1982). The detection of an extended structure in 0108+388 supports a hypothesis, in which old sources will appear as CSOs for a significant fraction of their life, because of their recurrent activity. CSOs provide a useful laboratory for the study of the physics of active galaxies at a very early stage of their activity. They also provide a unique probe of the interstellar medium within the inner part of the galaxy. Future multi-frequency global VLBI is planned to measure the expansion rates with respect to the cores and search for weak emission around CSOs.

People involved: I. Owsianik

Collaborators: J.E. Conway (OSO - Onsala Space Observatory), A.G. Polatidis (JIVE, OSO)

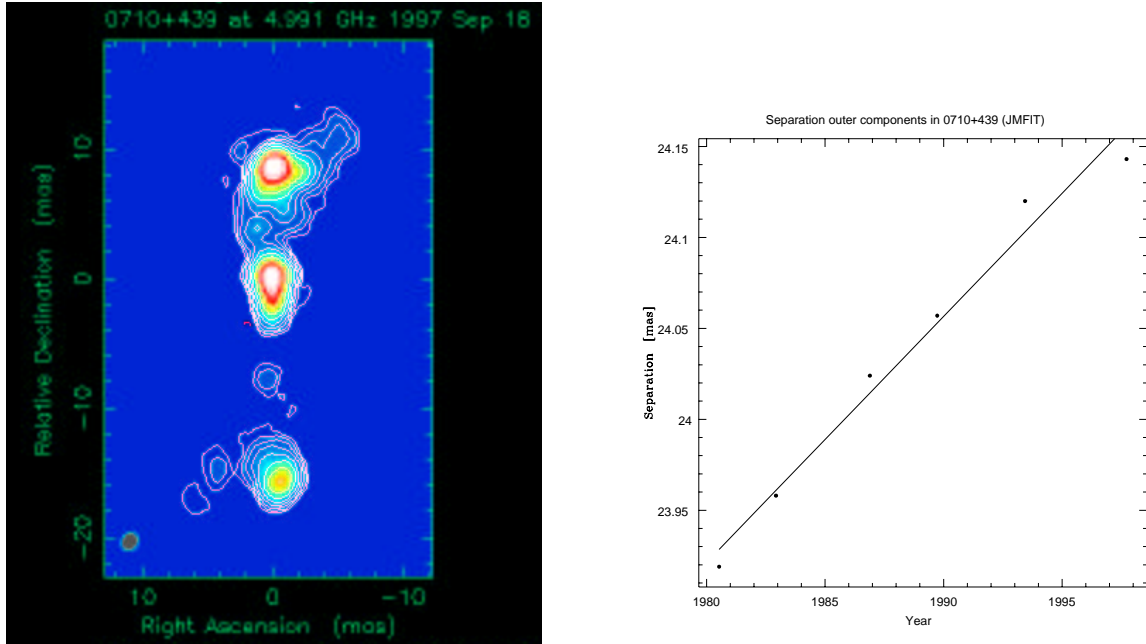


Figure 11: (left) VLBI 5 GHz map of 0710+439, rms noise=0.15 mJy/beam, (right) Separation vs. time of outer components, the fitted line corresponds to a separation velocity of $0.243 h^{-1} c$

3.5 Superluminal motion in the OVV quasar 3C454.3

At epoch ~ 1980 , a strong radio outburst began in the quasar 3C454.3 ($z=0.859$). Global VLBI observations thereafter at $\lambda 2.8$ cm revealed a complex structure in the core region, consisting of 3 stationary (but variable) components and weak features which appeared to recede from the core with velocities of $5\text{--}9c$. VLBI observations at $\lambda 6$ cm and 3.6 cm confirmed the presence of this superluminal feature (labelled “A” in Fig. 12), moving away from the core region along a curved path, with velocities ranging from $\sim 11c$ [1984–1985] to $\sim 22c$ [1985–1988.5] and then to $\sim 14c$ [1988.5–1991.9] (see also section 2.1).

Back extrapolation of the separation from the core indicates that this feature was ejected at epoch 1981 ± 1 , *i.e.* close to that of the radio outburst. Later epochs are being analysed and the source has been observed with VSOP at $\lambda 6$ cm.

People involved: I.I.K. Pauliny-Toth, J.A. Zensus

Collaborators: K.I. Kellermann (NRAO), G.D. Nicolson (NITR, RSA)

3.6 The BL Lac object 1803+784

The investigation of the S5–BL Lac source 1803+784 ($z=0.68$) was continued. In addition to the research on the kinematics of the mas-core region, mainly by means of mm and 3.6 cm VLBI, the overall structure of this unusually large D2 source was mapped using a “world array” consisting of the MERLIN interferometer and a global VLBI array. The 16 telescopes, used for 11 hours at 1.6 GHz, “filled” the uv-plane very densely.

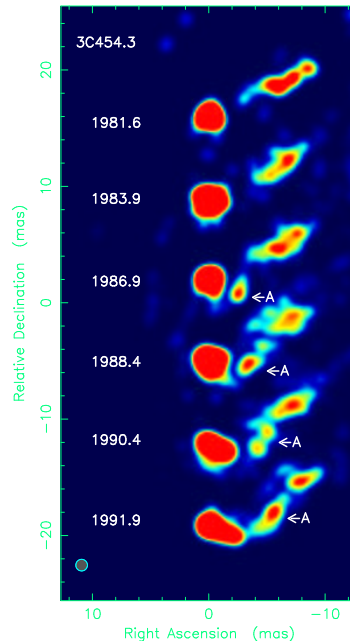


Figure 12: Images of 3C 454.3 derived from global VLBI observations at 5 or 8.4 GHz (last epoch). The restoring beam is 1 mas. The peak brightness temperatures range from $1.4 \cdot 10^{11}$ K (epoch 1990.4) to $4.1 \cdot 10^{11}$ K (epoch 1981.6, *i.e.* near the peak of the radio outburst at short cm wavelengths).

The emerging picture explains the vastly different position angles seen in the inner mas structure and the outer (1."5) component in terms of a spatially curved (probably helical) jet geometry. The inner part shows features moving superluminally along curved paths, also in agreement with the idea of a spatially curved, helical jet. The “transition point” between the EW (inner P.A.) and NS (outer P.A.) directions became, for the first time, convincingly visible in the new map.

People involved: A. Witzel, T.P. Krichbaum

Collaborators: S. Britzen (Dwingeloo), T. Muxlow (Jodrell)

3.7 Subparsec-scale structure in the core of 3C 111

Work has continued (see previous report) on 3C 111 ($z=0.0485$), a double-lobed FR II radio source associated with an N-type galaxy. The object contains a prominent superluminally variable pc-scale radio source with a one-sided jet pointing in the direction of the one-sided ‘VLA-jet’, and a broad line emission region embedded in a starlike nucleus.

3C 111 has the strongest compact core at cm/mm $\lambda\lambda$ ($S \gtrsim 1.5$ Jy) of all FR II radio galaxies, and at times it displays superluminal structural changes and/or strong mm-outbursts.

Following the large mm-outburst discovered with the IRAM interferometer in January 1996, the object was observed 4 times within 16 months with the VLBA plus the 100m telescope in the standard polarization mode at $\lambda 7$ mm, the first 2 times also simultaneously at

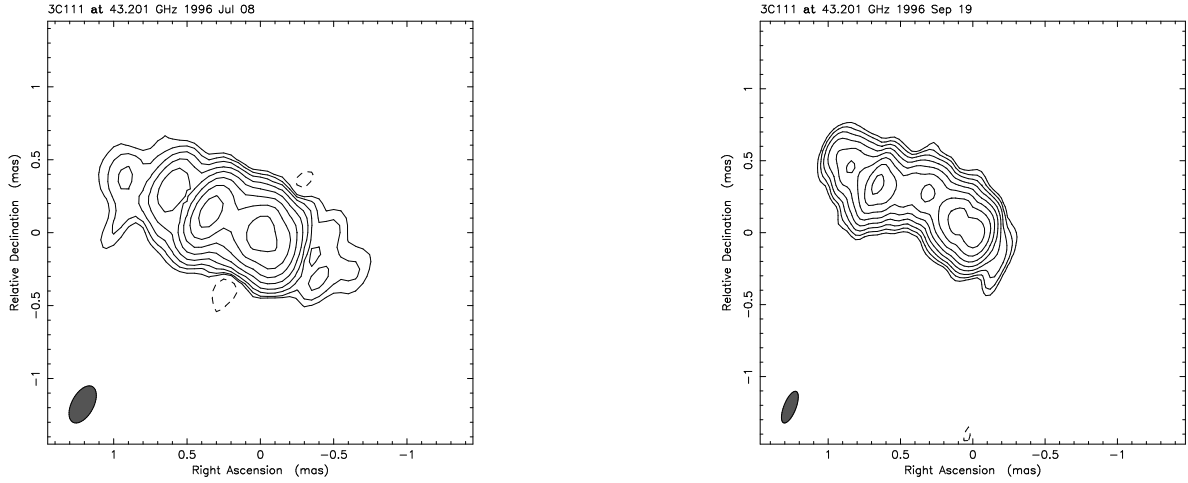


Figure 13: VLBI *clean maps* of 3C 111 at 43 GHz, at epochs 1996.5 and 1996.7. Contour levels are $-0.5, 0.5 \times 2^n$ % of peak brightness.

λ 3.6 cm. Preliminary total intensity maps at λ 7 mm (Fig. 13) show an elongated, curved multiple component structure ~ 1.1 mas in extent, roughly aligned with the large-scale jet. The structure is not of the common ‘core-jet’ type, there is no unresolved or strongly dominating component in these maps and the significant structural changes between the two epochs cannot be described by a simple kinematic pattern. To obtain a clearer picture of these changes, in the aftermath of the strong mm-outburst, more densely spaced observations are required. The 3.6 cm brightness distribution (first epoch; not shown here) shows a similar one-sided ‘core-jet’ structure as previous 6 cm maps. The polarized intensity map at 3.6 cm (same epoch) shows the brightest jet component, ~ 4 mas from the core, to be polarized at the 5% level (polarized flux density ~ 90 mJy).

People involved: W. Alef, E. Preuß

Collaborators: K.I. Kellermann (NRAO)

3.8 VLBI observations of very high redshift quasars

In a continuing investigation, ten quasars of extremely high redshift ($z > 3.1$) have been observed at 5 GHz either with a global VLBI array, or the EVN and the Hartebeesthoek antenna. The sample includes the most distant radio loud quasar known, 1428+123 with a redshift of 4.72. Most of the sources are well resolved and show asymmetric structure. The 3 most distant quasars ($z > 4$), however, are strikingly more compact than those at lower redshifts, *i.e.* they do not show jet-like structure in the VLBI maps. It is as yet not clear whether this is an intrinsic difference, or whether it is due to the high emitted frequency (for $\nu_{\text{obs}}=5$ GHz and $z > 4$, $\nu_{\text{em}} > 25$ GHz). Three high redshift quasars have also been observed at 1.6 GHz with VSOP; all are well resolved on HALCA baselines.

People involved: I.I.K. Pauliny-Toth

Collaborators: Z. Paragi (JIVE), S. Frey (FÖMI Budapest), K.I. Kellermann (NRAO),

R.T. Schilizzi (JIVE)

3.9 Seyfert galaxies

A sample of several Seyfert 2 galaxies has been observed with the HST and the VLA to study the influence of the radio ejecta of Seyferts on their Narrow-Line-Region (NLR). A detailed correspondence was found between features in the radio and emission-line images that clearly indicates strong interactions between the radio jets and the interstellar medium. Such interactions (see Fig. 14) play a major role in determining the morphology of the NLR, as the radio jets sweep up and compress ambient gas, producing ordered structures with enhanced surface brightness in line emission. $[\text{O III}]/(\text{H}\alpha + [\text{N II}])$ excitation maps have revealed bi-polar structures which can be interpreted as the ‘ionization cones’ expected in the unified scheme. This answers an old question: even though shock-ionization may not be the dominant source for the excitation of the NLR in AGN, the radio weak jets in Seyferts significantly influence the shape of this region.

People involved: H. Falcke

Collaborators: A.S. Wilson (Maryland), C. Simpson (Subaru Telescope)

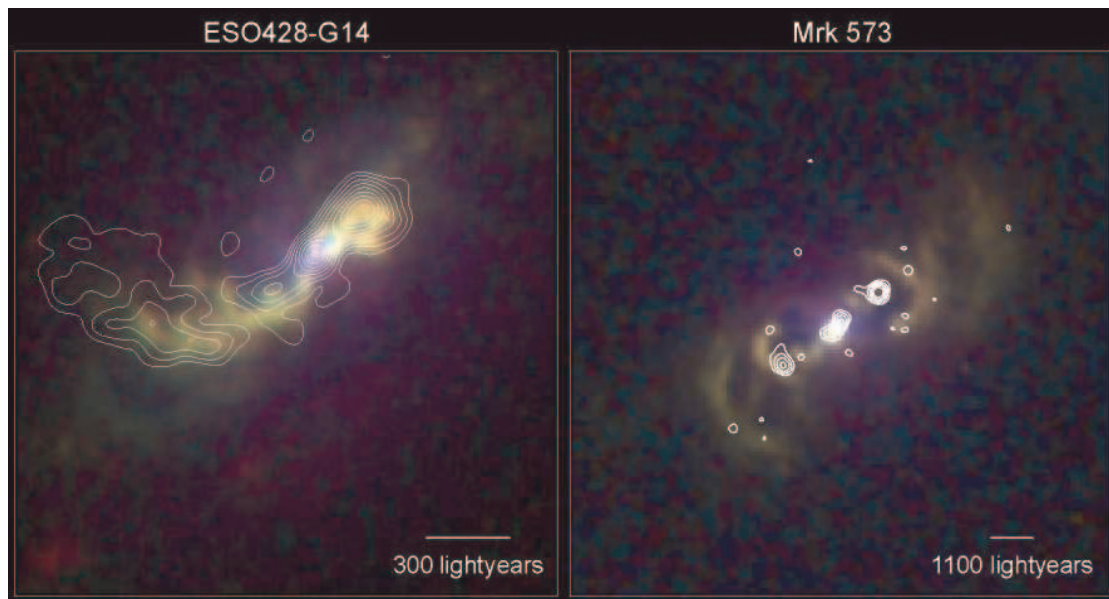


Figure 14: Deep images obtained with the VLA at 8 GHz are overlaid as contours on HST multi-color images of the NLR of two Seyfert 2 galaxies. In the HST images, red corresponds to $\text{H}\alpha$, green to $[\text{OIII}]$ and blue to the continuum. The NLR shows a highly ordered morphology with multiple strands and arches. Its correlation with the radio ejecta indicates that the morphology is mainly shaped by these; in ESO428-G14 probably through interaction between the ISM and the radio jet, while the ‘hotspots’ in Mrk573, where the jet is stopped in the ISM, produce bow shocks.

A few Seyfert galaxies have also been studied with VLBI, the VLBA and MERLIN. VLBI

multi-epoch observations of Mrk 348 and Mrk 231 have shown only sub-luminal motion, with $v = 0.073c$ and $v = 0.046c$ respectively, despite the relatively bright, variable compact radio source in them. Upper limits of $< 0.25c$ were established for NGC 4151 and NGC 5506. This suggests that Seyfert jets are either launched sub-relativistically or already slow down significantly on the sub-pc scale. This may help in understanding the difference between radio-loud and radio-quiet AGN.

Free-free absorption of emission from the nucleus by a putative surrounding torus was searched for with the VLBA at frequencies between 1.4 and 15 GHz in eight nearby Seyferts. A search for thermal emission from the ionised inner region of a torus (or accretion disc) has yielded one new candidate (NGC 4388).

People involved: H. Falcke, A. Roy, T.P. Krichbaum

Collaborators: K.R. Anantharamia, W.M. Goss, J.F. Herrnstein, J.S. Ulvestad, M.A.W Verheijen, J.M. Wrobel (NRAO), C.G. Mundell, A.S. Wilson (Maryland), L.J. Greenhill, J.M. Moran (CfA), E.J.M. Colbert (GSFC), C.G. DePree (Agnes Scott College), P.J. Diamond (Jodrell), T.A. Osterloo (NFRA)

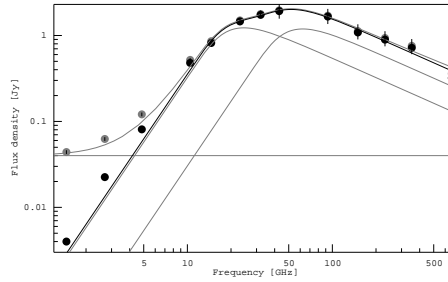


Figure 15: Radio spectrum of III Zw 2. Gray dots show flux densities measured in May 1998, black dots show the outburst spectrum with the quiescent level of 40 mJy (measured in 1995 at 8 GHz) subtracted. The three, gray dotted lines represent the three fitted components (quiescent level and two self-absorbed synchrotron components), the black solid line is the resulting fit to the outburst spectrum (self-absorbed synchrotron components only) and the gray dashed line represents the fit to the total observed spectrum. The two-component-model was confirmed by 7 mm VLBI observations.

In early 1998, the onset of a major flare was detected in the spiral Seyfert galaxy III Zw 2 and its evolution was monitored. The flare peaked at mm- λ and showed the most inverted spectrum of any compact radio core known. The spectral index was $\alpha = +2$ before, and $\alpha = +2.5$ after subtraction of the quiescent level (Fig. 15). This confirms some basic predictions of synchrotron theory since it was possible to determine a size ($50 \mu\text{as}$) and a structure (compact double) with VLBI at λ 7 mm that matched exactly the parameters derived from the spectral fitting. This is probably the most extreme outburst so far seen, with an increase in flux of more than a factor 30 within 2 years. The monitoring of this event will be continued.

People involved: G. Bower, H. Falcke, A.P. Lobanov, T.P. Krichbaum, A. Patnaik, A. Brunthaler (diploma thesis)

Collaborators: *M.F. Aller, H.D. Aller (Michigan), H. Teräsranta (Metsähovi), M.C.H. Wright (Berkeley), G. Sandell (NRAO)*

The TeV X-ray flare of Mrk421 observed in May 1994 was interpreted in terms of the synchrotron-self-Compton (SSC) mechanism. It is suggested that the flare may have been produced by a high-energy component with a flatter energy distribution and a higher energy-cutoff than the quiet component, which only radiates in the soft X-ray to radio bands.

People involved: *A.P. Lobanov, H. Falcke, T.P. Krichbaum, A. Kraus, A. Witzel*
Collaborators: *H. Meyer (Univ. of Wuppertal), E. Lorenz (MPP, Muenchen)*

3.10 Sagittarius A*-like objects

The VLA has been used at 15 GHz to search for Sgr A*-like radio-cores in other nearby, weakly-active galaxies. Two samples have been derived from the Palomar sample (ApJS 98, 477, 1995): a) a sample of 48 nearby LINER galaxies, and b) a sample of the 100 closest AGN of all types found with the Palomar 5 m telescope.

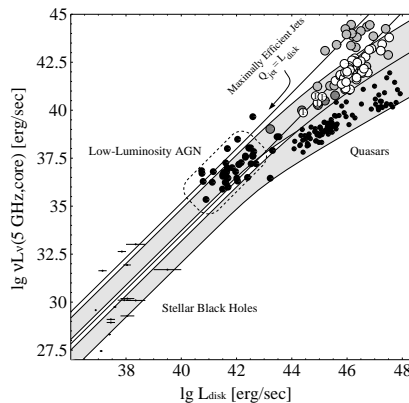


Figure 16: Correlation between accretion disk luminosity L_d (*i.e.* nuclear optical+UV luminosity for AGN) and radio core luminosity L_ν at 5 GHz. The shaded bands are the theoretical predictions for L_ν as a function of L_d for relativistic jets with randomly oriented inclination angles. The radio cores of the newly added LINER galaxies are given by big dots, quasars are given by open (steep-spectrum, radio-loud) and filled (flat-spectrum, radio-loud) circles, as well as smaller dots above $L_d = 10^{44}$ erg/sec (radio-quiet). Sources in the lower left are Sgr A*, M31* and black holes of stellar mass.

The survey has revealed the presence of a compact radio core in a quarter of all sources. The cores seem to be correlated with the optical activity. Follow-up VLBA observations of the brightest sources give brightness temperatures $> 10^8$ K for these cores, thus confirming their AGN nature—at least for some of the LINERs the AGN nature has been questioned so far. The correlation found between optical and radio luminosity falls exactly on the predictions from the jet/disk-symbiosis model published earlier (Fig. 16). The two brightest radio cores also show extended jet-like structures on VLBI scales and the flat spectral indices of all cores

also suggest a jet nature rather than emission from an Advection Dominated Accretion Flow. This suggests that the common-engine mechanism (Nat 349, 138, 1991) does extend to AGN at much lower powers.

People involved: H. Falcke

Collaborators: A.S. Wilson, N. Nagar (Maryland), L.C. Ho (Carnegie), J. Ulvestad (NRAO)

4 Gravitational lenses

The gravitational lens effect occurs when the gravitational field of an intervening object (galaxy) distorts the radiation from a distant object. Typically, 2 or 4 detectable images are produced, each of which is a scaled and distorted image of the background source. VLBI polarimetry provides a powerful tool for investigating gravitational lens images, since the degree and angle of linear polarisation are unchanged by the lens process itself. This provides a constraint on the mass distribution of the lensing object. Quadruple ("Quad") systems are of particular interest, since they provide magnifications of intrinsic motions in the source by factors of 10–100.

4.1 The image morphology of the gravitational lens 2016+112

MG 2016+112 has long been a puzzle; at both radio and optical wavelengths there are at least 2 images, but the nature of a third, elongated radio source in the system has been unclear.

Observations were made with the EVN at 5 GHz in 1995, in phase-referencing mode, since the source is weak at this frequency. The two known image components (A and B) were resolved with the 5 mas beam, each showing the double structure of the background object. The third region (C) is revealed to be composed of 4 distinct components, spaced along a gently curving arc (Fig. 17, right panel). Comparison with previous 1.6 GHz EVN results strongly supports a model in which C consists of 2 further, almost "merging" images of the background double source. Because of the combined effects of a spectral difference between the two components of the background source, and strong differential lens magnification in region C, the integrated spectra of A and B differ significantly from that of C.

People involved: R.W. Porcas, A. Patnaik

Collaborators: M. Garrett (Jodrell, JIVE), S. Nair (Jodrell, RRI Bangalore)

4.2 VLBI Studies of the Quad Gravitational Lenses PKS 0411+05 and QSO 1422+231

From VLBI data, it should be possible to measure motions between the quad components produced by changes in the alignment of the system observer-lens-background object in a ~ 3 yr programme. The quads PKS 0411+05 and QSO 1422+231 were observed in November 1997 and June 1999 using a sensitive global array, to detect such proper motions and high-quality VLBI images of both radio sources were obtained. Fig. 17, left, shows the wide-field

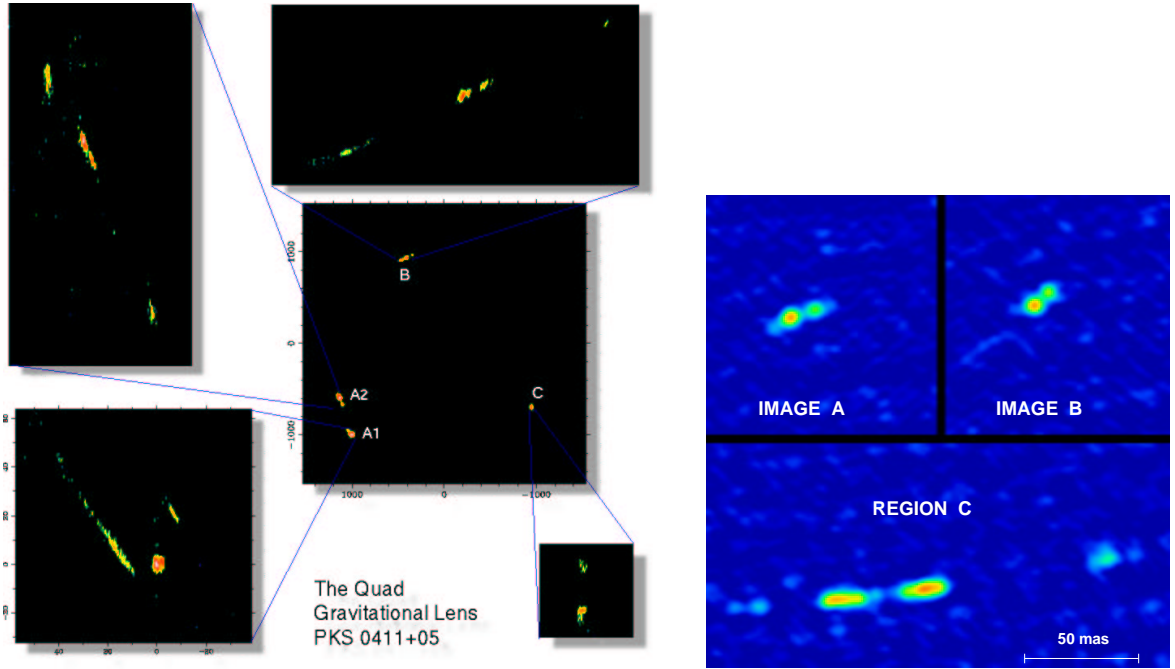


Figure 17: **Left 5 panels:** Results of the 8.4 GHz VLBI mapping of the quad gravitational lens PKS0411+05. The synthesized beam for the images is of 1.8×0.6 mas/beam (P.A. -6°). **Right panel:** EVN 5 GHz maps of the gravitational lens system 2016+112. Beam 6×6 mas; peak brightness 6.6 mJy/beam.

imaging results for the first epoch of observations of PKS0411+05, which displays extended structures in the four lensed sub-images.

Positions and flux densities alone are not enough to produce unique lens models of quads (which are produced by elliptical gravitational potentials). The location of subcomponents obtained from this mapping can provide crucial information for distinguishing between different lensing models. With the data obtained and observations at further epochs it will be possible to improve the lens modelling and detect any changes in the structure of the quads, in their relative positions, etc.

People involved: E. Ros

Collaborators: J.M. Marcaide J.C. Guirado, M.A. Pérez-Torres (Universitat de València, Spain), L.J. Lara, A. Alberdi (IAA-CSIC, Granada, Spain)

4.3 VLBI Polarimetry of gravitational lens systems

VLBI polarisation observations have been made of the lens 0218+357, using the VLBA at 43 GHz, and the VLBA + Effelsberg at 8.4 GHz. Both images in this system show 2 components, in A separated by 1.38 mas in PA 51° , in B by 1.47 mas in PA 90° . The western, more compact, component in each image appears to be the "core". The 8.4 GHz observations show this to be the most highly polarised component in both images; the observed polarisations angles differ, however, as a result of the large difference in Faraday rotation along the 2 image

paths. At 43 GHz, the Faraday rotation is negligible, and the polarisation angles are the same, confirming that the lens action itself does not change the polarisation angle, despite the very different structural position angles in the A and B images. Polarisation VLBI observations of other gravitational lens systems have also been made recently, using the VLBA and Effelsberg, and analysis of 5 GHz observations of 0218+357 is currently underway.

Analysis has recently been made of 8.4 GHz observations of the 4-image system 1422+231 (see also 4.2). All 4 images are detected, and the distribution of polarised emission has been mapped in the 3 stronger ones. The two strong images, A and B, show the characteristic "tangential stretching" of the intrinsic source structure, resulting in elongated, but relatively featureless morphologies. In contrast, the polarised emission exhibits a number of sub-features in the images, including a change of polarisation angle along the image extent. This feature enables one to identify corresponding regions in the images, and demonstrates the opposite parities of A and B, which is barely apparent from the total intensity distributions alone. There is a systematic difference of $\sim 20^\circ$ between the polarisation angles of the A and B images, which can be attributed to differential Faraday rotation along the two image paths.

People involved: R. W. Porcas, A. Patnaik

Collaborators: A. Kembal (NRAO)

5 Astrometry and phase-referencing

The corruption of the phase in VLBI observations causes information about the absolute position of radio sources to be lost. This lost information can be partially recovered using phase-referencing techniques. Having strong sources (in a known reference frame) near the target source, it is possible to reference the position of the latter to the former, by transferring the interferometric phase from the reference source to the target source. The phase-connection process has been carried out for sources separated by as much as 15° , giving a sub-mas precision in the separation determination. By combining different epochs of phase-referencing observations, it is possible to register different images unambiguously and measure the proper motions of radio source components.

5.1 High precision differential astrometry

The VLBI technique can determine astrometrically relative positions with sub-mas accuracy. The technique of phase-delay differential astrometry has been applied to different groups of radio sources. The pair 1928+738/2007+777 of $4.6''$ separation was studied, with the addition of 1803+784, to take advantage of the constraints introduced by a triangular geometry in the determination of the angular separations. For such observations, the ionospheric contribution to the observables was modelled using ionospheric total electron content (TEC) information derived from GPS data. Comparison with previous epochs made it possible to determine unambiguously the position of the core of 1928+738 and also the proper motions of components in this radio source. The phase-connection over a separation as large as 15° has also been tested in the pair 1150+812/1803+784.

After these successful astrometric observations, it became possible to extend the high pre-

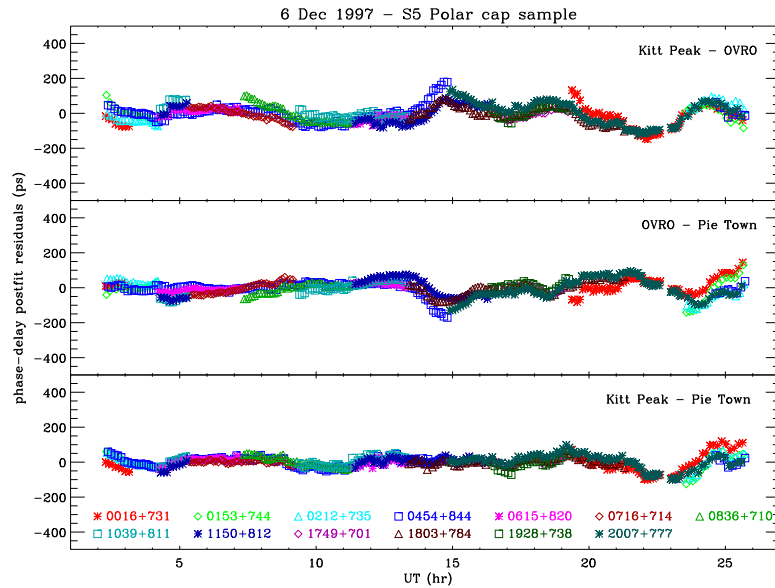


Figure 18: Preliminary results of the first epoch of 3.6 cm observations of the complete S5 polar cap sample: postfit residuals of the (undifferenced) phase-delays after a weighted least-squares analysis which estimates the relative separations among the radio sources. One phase-cycle at the frequency of 8.4 GHz corresponds to 120 ps of phase-delay. Notice a similar trend for all sources. Those trends cancel out in the differences to yield a global residual rms of only 30 ps.

cision differential astrometry to a larger set of radio sources, *e.g.* the S5 polar cap sample of 13 sources. An astrometric programme was begun on all the members of this sample with a first epoch in 1997.93. Further measurements at 8.4 GHz were made at epoch 1999.41 and at 15 GHz in late summer 1999. All phase-delay data from the first epoch were connected and the performance of the station clocks was modelled to high accuracy to obtain a global solution of all the positions. The undifferenced postfit phase-delay residuals of this preliminary work are shown in Fig. 18. The astrometric observations of this set of radio sources over 5 years will provide a precision in the relative separations and component proper motions in the radio sources better than 0.1 mas, the most precise to date.

People involved: E. Ros

Collaborators: J.M. Marcaide, J.C. Guirado, M.A. Pérez-Torres (Universitat de València, Spain)

5.2 Phase reference study of a weak core close to the quasar 1636+47

The analysis of data for this source (see previous report) has been completed. The 1.5 mas resolution Global VLBI map of 1636+47A reveals an extended core and a weak jet component in P.A. -30° which together account for 95% of the total flux seen in contemporaneous MERLIN data. The phase-referenced map of B shows an unresolved core with peak flux 6.7 mJy. It proved possible to improve the dynamic range of this map by phase self-calibration (since Effelsberg and the phased-VLA provided high-sensitivity elements in the Global array). The

hybrid map revealed a faint extension of ~ 2 mJy, in P.A. 90° , in the direction of the faint arcsec-scale jet seen in the MERLIN map of B. The total flux of the core-jet in this map increased, indicating the extent to which phase-reference “coherence losses” reduce the quality of the phase-referenced image; some 95 % of the total MERLIN core flux is contained in the hybrid map.

People involved: R.W. Porcas

Collaborators: M. Rioja (JIVE)

6 Variability

Studies of the variability of radio sources and, in particular, of Intraday variability (IDV) on time scales shorter than one day, provide important clues as to the size of the emitting region(s) and the mechanisms involved.

6.1 Intraday Variability

Even more than ten years after its discovery, the phenomenon of IDV of blazars is still puzzling. The complete subsample of flat-spectrum sources of the 1-Jy-catalog with $\delta \geq 50^\circ$ (35 objects) has now been investigated for IDV. About 1/3 of all blazars observed (73 sources) show variations on timescales of less than 2 days with amplitudes ranging from a few % up to more than 20 % in selected objects. The analysis of the observations made with the 100m telescope showed that usually the variations in total flux density are accompanied by those in linear polarization (polarized flux density and polarization angle). Variations of the polarized flux density are in most cases larger than those of the total flux density and can reach a factor of 2 (*e.g.* in 0917+624). The polarization angle can vary from a few degrees up to 100° . As an example, the light curve of the strongly variable quasar 0917+624 which was observed in December 1997 at two frequencies, is shown in Fig. 19.

These quasi-periodic variations on a 10–15 %-level were typical for this source during all observations made since 1985. Amazingly, in February 1998, only a monotonic increase (by about 7%) during a five-day observing campaign was seen. In a more recent observation (in February 1999), the source seems to have returned to its “usual” variability state. This significant change in the variability characteristics of this source should be of help in gaining more insight into the IDV-phenomenon.

In the case of an intrinsic origin of the variations the brightness temperature can be derived from the the light-travel-time argument and standard synchrotron formulae; for $\lambda = 6$ cm this yields $T_B \simeq 3 \cdot 10^{18}$ K, far in excess of the inverse-Compton limit. However, owing to the small source sizes involved, a contribution of interstellar scattering to the observed variations is highly probable. We note that Intraday variability is also observed in all other domains of the electromagnetic spectrum.

People involved: A. Kraus, A. Witzel, T.P. Krichbaum, S.J. Qian

Collaborators: A. Quirrenbach, B.J. Rickett (UCSD), S.J. Wagner (LSW, Heidelberg)

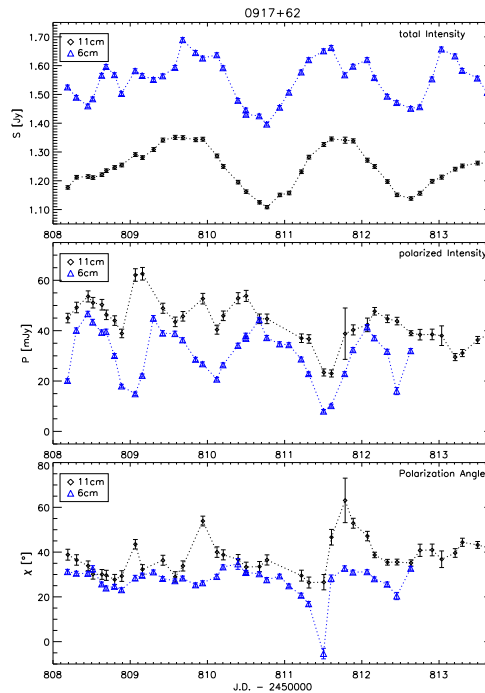


Figure 19: IDV in the QSO 0917+624 in total intensity and linear polarization at two wavelengths: λ 11 cm (diamonds) and 6 cm (triangles). The data has been shifted by a small amount for better visibility. The variations of the total and the polarized intensity are anti-correlated; this is clearly visible at least at 6 cm.

In a theoretical investigation, the multifrequency polarization behaviour of the IDV-event observed in May 1989 at five frequencies (1.4, 2.7, 4.9, 8.3 and 15 GHz) in 0917+624 (see above) has been analysed. It was shown that this behaviour is highly wavelength dependent and that the variations at 1.4 GHz are mostly due to refractive interstellar scintillation. The proposed scintillation model fits the 1.4 GHz lightcurves of the total and polarized flux density and polarization angle very well. But after subtracting the variations due to scintillation there are two significant minibursts in the polarized flux density lightcurve, which are well correlated with the variations at the four higher frequencies and they have almost the same timescale (~ 0.3 days). It is suggested that both the 1.4 GHz minibursts and the intraday variations at the higher frequencies are mainly of intrinsic origin. This is the first time that it has been possible to distinguish the intrinsic variations from the scintillation in this source. A shock model has also been proposed to explain the complicated intraday polarization behaviour at the higher frequencies.

People involved: S.J. Qian, A. Kraus, A. Witzel, T.P Krichbaum, J.A. Zensus

6.2 Multifrequency monitoring of selected blazars

Since late 1996, a monitoring program has been carried out, on a roughly monthly basis, of selected blazars (mostly those which are active in the high-energy range or showed pronounced intraday variations in the past). Use was made of the unique ability of the 100m telescope of

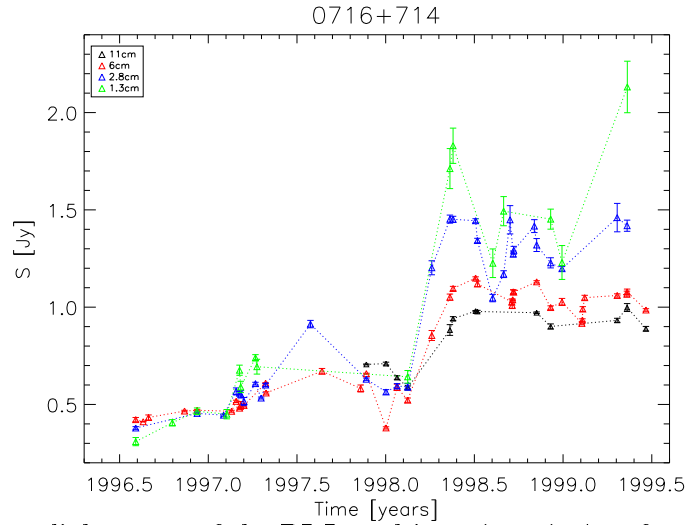


Figure 20: Long-term light curve of the BL Lac object 0716+714 at four wavelengths: 11 cm, 6 cm, 2.8 cm, and 1.3 cm.

switching between (up to 8) receivers in the secondary focus within about 30 seconds. This results in a good spectral coverage, although the observations are often confined to a smaller number of receivers because of poor weather or technical reasons. As an example the long-term light curve of the BL Lac object 0716+714 is shown in Fig. 20.

At the four most frequently used wavelengths ($\lambda = 11, 6, 2.8, 1.3$ cm), pronounced variability and a strong outburst in mid-1998 are seen. The theoretical interpretation of the data is underway. In the case of the γ -ray active quasar 0836+710 it was possible to connect a radio outburst to a γ -flare and the birth of a new VLBI component (see also 2.1, 2.4).

People involved: A. Kraus, A. Witzel, T.P. Krichbaum, A.P. Lobanov, B. Peng

An unusual event of rapid flux density variations with a timescale of ~ 4 days, observed at 1.49, 4.86 and 8.44 GHz in the highly variable BL Lac object AO0235+164, has been analysed. It was shown that its distinct properties (the delay between the burst maxima at 4.86 and 8.44 GHz and that at 1.49 GHz, and the decrease of the burst duration with increasing wavelength) can be interpreted in terms of an relativistic aberration model, in which a thin shock moves with a large Lorentz factor ($\Gamma \gtrsim 25$) along slightly curved magnetic field lines in the jet.

People involved: S.J. Qian, A. Kraus, A. Witzel, T.P. Krichbaum, J.A. Zensus